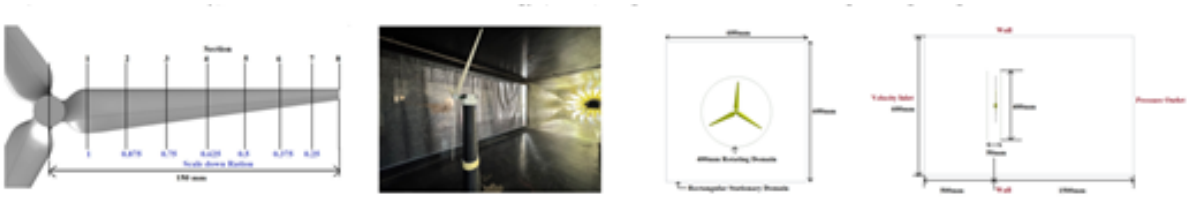
Ceylon Journal of Science 55 (4) 2026: 1661-1674

RESEARCH ARTICLE

Application of Passive Trailing Edge Morphing for Aerodynamic Enhancement of HAWT Blades under Low Reynolds Number Conditions

Siddalingappa P. Kodigaddi, A.R. Keven and A. Ahmed

Graphical Abstract

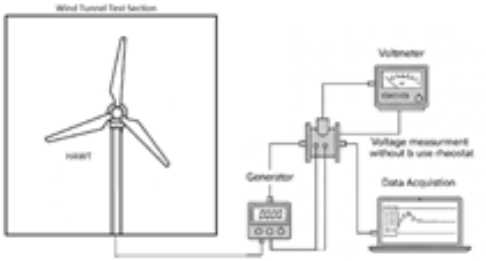


Sectional Dimensions

HAWT in WT

Domain for CFD analysis

- Baseline small-scale HAWT blade using **NACA 2412 airfoil**
- Trailing edge morphing applied at **50% chord**
- Deflection cases analyzed: **5°, 10°, 15°**
- Low Reynolds number performance evaluated using **CFD (k–ε + MRF)** and **wind tunnel experiments**
- Morphing improves lift characteristics and delays flow separation
- Coefficient of power increases across operating TSR range
- **15° deflection delivers optimum performance**
- Maximum **46.5% improvement in Cp at TSR = 6**
- Validated agreement between numerical & experimental results (<10%)
- Confirms trailing edge morphing as an effective solution for **low-wind / small-scale HAWT efficiency enhancement**



Schematic of experimental setup

Highlights

- Proposes passive trailing-edge morphing at 50% chord for small-scale HAWT blades
- Evaluates +5°, +10°, and +15° trailing-edge deflections at low Reynolds numbers
- Combines k–ε-MRF simulations with experimental validation using a 350-mm HAWT prototype
- Demonstrates improved power coefficients across most tested tip-speed ratios
- Achieves a maximum power increase of 46.5% at a TSR of 6.0 with +15° deflection

Ceylon Journal of Science 55 (4) 2026: 1661-1674
DOI: https://doi.org/10.4038/cjs.v55i4.9656

RESEARCH ARTICLE

Application of Passive Trailing Edge Morphing for Aerodynamic Enhancement of HAWT Blades under Low Reynolds Number Conditions

Siddalingappa P. Kodigaddi*, A.R. Keven and A. Ahmed

Nitte (Deemed to be University), Nitte Meenakshi Institute of Technology (NMIT), Department of Aeronautical Engineering, Bengaluru – 560064, India

Received: 03.03.2026 Accepted: 16.09.2026

Abstract

This study investigates the enhancement of the aerodynamic performance and efficiency of horizontal-axis wind turbine (HAWT) blades through passive trailing-edge morphing. The novelty of this work lies in the application of substantial trailing-edge deflection at 50% chord to a NACA 2412 airfoil for HAWT applications. The effects of three deflection angles (+5°, +10°, and +15°) were investigated numerically and experimentally under low-Reynolds-number operating conditions. Numerical analyses, conducted using the k–ε turbulence model and the multiple reference frame (MRF) approach, were complemented by experimental validation using a 350-mm-diameter HAWT prototype in a low-speed wind tunnel. The primary objective was to assess the influence of trailing-edge morphing on the coefficient of power, flow characteristics, and surface pressure distributions. The results show that the coefficient of power generally increases with the tip-speed ratio (TSR) within the optimal operating range before declining at higher TSRs. Importantly, trailing-edge deflection significantly enhanced the coefficient of power across most TSRs, with the +15° deflection consistently yielding the highest performance in both the numerical and experimental analyses. The numerical and experimental coefficient-of-power values agreed within 10%, while the blade with a +15° trailing-edge deflection demonstrated a substantial 46.5% increase in performance relative to the straight blade at a TSR of 6.0. These findings demonstrate that passive trailing-edge morphing is a promising approach for improving the aerodynamic efficiency of small-scale HAWTs, particularly under low-Reynolds-number operating conditions.

Keywords: Aerodynamic Performance; Computational Fluid Dynamics (CFD); Horizontal Axis Wind Turbine (HAWT); Low Reynolds Number; Multiple Reference Frame (MRF); Trailing Edge Morphing

INTRODUCTION

The rising global demand for sustainable energy has accelerated the development of renewable technologies, with wind energy emerging as a leading sector. HAWTs remain the dominant choice in large-scale wind power generation due to their proven efficiency and technological maturity (Ameduri & Concilio, 2020; Apata & Oyedokun, 2020; Barbarino et al., 2011; Manwell et al., 2010; Nabhani et al., 2025; Tummala et al., 2016). However, consistently high performance across fluctuating wind speeds, especially at low Reynolds number conditions typical of small-scale turbines or during low-wind scenarios for larger systems, continues to present a critical challenge (Akhter & Omar, 2021; Roslan et al., 2022; Saemian & Bergadà, 2025; Temesgen Terefa et al., 2025; Yan et al., 2019).

Traditional HAWT blades utilize fixed geometries optimized for rated wind speeds, resulting in limited adaptability and suboptimal energy capture under off-design conditions. Although pitch control mechanisms provide some flexibility, their complexity, inertia, and inability to address spanwise performance issues restrict their efficacy. Recent engineering focus has shifted toward advanced blade adaptation strategies, inspired by biological morphing techniques and aimed at real-time aerodynamic optimization (Ajaj et al., 2016; Bi et al., 2020; Khedr, 2025).

Morphing technology, particularly trailing edge morphing, enables dynamic modification of blade camber, directly influencing lift and drag characteristics (Huang et al., 2019; Maguire et al., 2024; O'Brien et al., 2017; Parancheerivilakkathil et al., 2024; Saemian & Bergadà, 2025). Adjusting trailing edge deflection alters the effective angle of attack, which can maintain optimal operating

*Corresponding Author's Email: siddalingappa.pk@nmit.ac.in
https://orcid.org/0000-0001-5712-4555

This article is published under the Creative Commons Attribution License (https://creativecommons.org/licenses/by/4.0/), which permits unrestricted use, distribution, and reproduction in any medium, provided the original work is properly cited.

states and significantly mitigate flow separation especially at low Reynolds numbers (Akhter et al., 2023; Chen & Qin, 2017). Prior studies have demonstrated improved aerodynamic performance and lift-to-drag ratios for airfoils with trailing edge morphing (Cheng et al., 2023; Clements & Djidjeli, 2023; Douglas et al., 2019; Kan et al., 2020; Kodigaddi, 2026; Kodigaddi et al., 2026; Kodigaddi & Venkataramana, 2025; Wang et al., 2023).

Complementary passive strategies, such as surface dimpling, have shown promise in further delaying flow separation and reducing drag in low Reynolds number regimes. The addition of dimples induces turbulence in the boundary layer, helping sustain attached flow and enhancing blade efficiency (Arunvinthan et al., 2021; Mohammadi & Maghrebi, 2020). However, the interplay between trailing edge morphing and dimpled surfaces in HAWT blade design remains insufficiently explored, particularly at critical trailing edge regions (Li & He, 2023).

Despite incremental advancements, there is a clear gap concerning the use of morphing and tailored geometric modifications under low Reynolds number conditions for HAWT blades. Prior research largely investigates these strategies in isolation, without addressing their synergetic effects or validating their utility for small-scale, low-wind turbines. While trailing edge morphing at extended chord lengths has been previously reported (Zhuang et al., 2020), its application to small-scale horizontal axis wind turbines operating under low Reynolds number conditions remains relatively limited. The present study addresses this gap by combining detailed CFD analysis with experimental validation to assess aerodynamic performance over a range of tip speed ratios. Using a NACA 2412 airfoil as the baseline, trailing edge morphing up to 50% chord is investigated for deflection angles of +5°, +10°, and +15°, with a focus on improving performance in low-wind regimes where flow separation and reduced lift significantly affect turbine efficiency.

The primary objective of this work is to enhance both the aerodynamic performance and efficiency of HAWT blades by applying passive trailing edge morphing on a NACA 2412 airfoil. The focus is on quantifying the effects of three different trailing edge deflection angles under low Reynolds number conditions, aiming to improve coefficient of power and overall energy capture relative to conventional blade designs (Kodigaddi et al., 2022; Kodigaddi et al., 2026; Kodigaddi & Venkataramana, 2025). Preliminary results demonstrate that the proposed morphing strategy achieves meaningful improvements in coefficient of power compared to non-morphing blades. The approach supports more flexible and responsive blade operation across changing wind conditions, confirming its value as a promising solution for optimizing energy output in small-scale and low-wind HAWT applications.

The structure of the paper includes the methodology section concisely described the selection of the base airfoil and outlined the blade design process, detailing the setup for both CFD analysis and experimental wind tunnel testing. It also included a mesh independence validation to ensure numerical accuracy. The results and discussions presented a comparison of key numerical and experimental outcomes, focusing on pressure, velocity, turbulence, surface pressure, streamlines, and coefficient of power improvements observed with various morphing configurations. The conclusion summarized the primary findings, emphasized the significant aerodynamic gains achieved through passive trailing edge morphing, discussed the close agreement between CFD and experimental results, and highlighted opportunities for future research in adaptive wind turbine blade design.

MATERIALS AND METHODS

Airfoil selection

The NACA 2412 airfoil, with its 2% camber at 40% chord and 12% thickness-to-chord ratio, was selected for this study due to its proven aerodynamic efficiency, lift generation at low angles of attack, structural robustness, gradual stall behaviour, and extensive data availability, making it a reliable foundation for integrating advanced features like trailing-edge morphing in HAWT blades (Kassa et al., 2024). Aerodynamic enhancement was further achieved through controlled trailing edge deflection starting from the 50% chord, where three configurations +5°, +10°, and +15° deflection were examined to improve performance, particularly under low wind speed conditions where traditional blades underperform (Giammichele et al., 2024; Kodigaddi et al., 2025; Mowla et al., 2025). The parabolic morphing of the trailing edge was adopted and modeled as shown in Figure 1 (Douglas et al., 2019; Kaul & Nguyen, 2015). CFD simulations were conducted for each configuration to determine the optimal deflection angle that maximizes energy capture while maintaining mechanical feasibility. Wind turbine performance was assessed with reference to the Betz limit (Kulak et al., 2024), the present research encompasses a comprehensive analysis using multiple test cases as detailed in Table 1. Where ω is angular velocity in rad/s.

Blade design parameters

For experimental validation, the full-scale design was scaled down by a factor of three, resulting in prototype blade lengths of 150 mm and a rotor diameter of 350 mm. A uniform 3° pitch angle and passive trailing edge deflections (+5°, +10°, +15° from 50% chord) were employed to maintain favourable angle of attack, enhance camber-induced lift, and delay stall (Kodigaddi & Venkataramana, 2025; Li et al., 2025; Sudhamshu et al., 2016). This scale was selected to align with laboratory constraints while preserving aerodynamic similarity through proper scaling techniques (Burdett & Van Treuren, 2012). The design employs a linear scaling approach across seven sections: Section 1 remains at full scale (1.0), while Sections 2 through 7 are successively reduced by a scale factor of 0.125 relative to the preceding section.

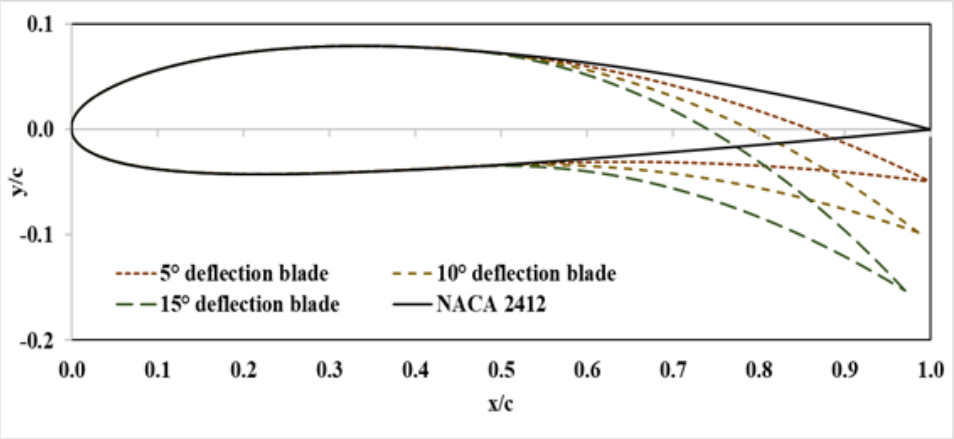


Figure 1: Comparison between the NACA 2412 and Trailing edge morphed at +5°, +10° and +15° deflection angles

Table 1: Test cases considered for both numerical and experimental studies

Target TSR	ω @ V=2 m/s (rad/s)	ω @ V=3 m/s (rad/s)	ω @ V=4 m/s (rad/s)	ω @ V=5 m/s (rad/s)
1	11.429	17.143	22.857	28.571
2	22.857	34.286	45.714	57.143
3	34.286	51.429	68.571	85.714
4	45.714	68.571	91.429	114.286
5	57.143	85.714	114.286	142.857
6	68.571	102.857	137.143	171.429
7	80	120	160	200
8	91.429	137.143	182.857	228.571

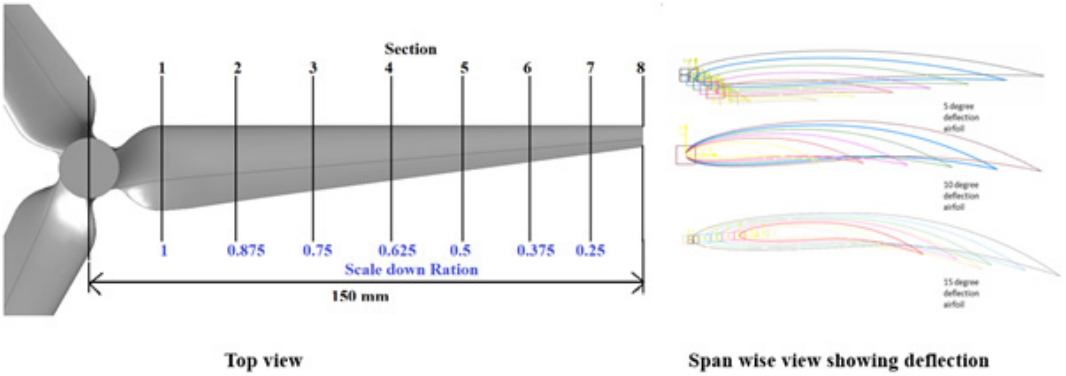


Figure 2: Sectional dimensions of the scaled HAWT blade prototype

This results in Section 7 having a scale ratio of 0.25, as illustrated in Figure 2.

Computational domain and boundary conditions

The geometric model was constructed using ANSYS Workbench 2024 R2 Design Modeler for low Reynolds number analysis. A cylindrical rotating domain with a diameter of 400 mm was created to enclose the HAWT rotor, extending 50 mm axially both upstream and downstream to capture critical near-field aerodynamic effects. This rotating region was embedded within a larger rectangular stationary fluid domain with dimensions 600 mm × 600 mm in cross section, extending 500 mm upstream and 1500 mm downstream to allow for complete wake development and minimize domain-induced effects. The overall computational setup, including both rotating and stationary zones, is illustrated in Figure 3. Boolean operations were used to isolate the rotating and stationary domains, and named selections were applied to define boundaries and interfaces for accurate mesh generation and solver assignment. The domain was discretized using unstructured tetrahedral elements, with refined meshing around the rotor blades to resolve complex boundary-layer behaviour and wake structures. A detailed view of the meshing strategy in the entire domain and a zoomed region around the rotor is shown in Figure 4.

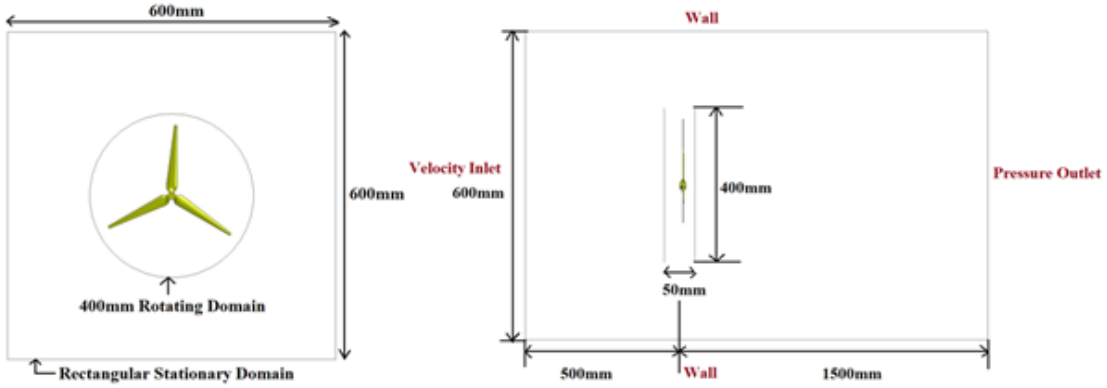


Figure 3: Computational domain setup: (a) front view and (b) side view

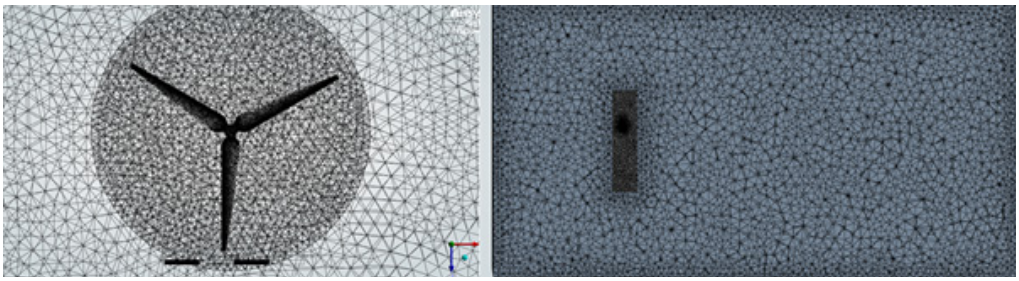


Figure 4: Meshing: (a) around the blade and (b) fluid domain

To simulate the aerodynamic performance, a uniform velocity inlet boundary condition was imposed at the upstream face, specifying a constant freestream velocity with 5% turbulence intensity and a turbulent viscosity ratio of 10. A pressure outlet with a static gauge pressure of 0 Pa was assigned at the downstream boundary. Convergence was set to 10^3 for all equations. To solve the turbulent flow near the airfoil surface or wall, the y^+ predicted through first spacing = 0.03 mm is 0.9893 and it is sufficient to achieve turbulent flow near the airfoil surface (wall) ($y^+ < 1$) (Somashekar & Immanuel Selwynraj, 2022). All solid surfaces, including the rotor blades, hub, and domain walls, were modelled as no-slip walls. For turbulence modeling, the k-epsilon (k-ε) turbulence model was selected due to its robustness, computational efficiency, and proven accuracy in simulating a wide range of internal and external flow problems (Daróczy et al., 2015; Mane et al., 2025). The cylindrical region enclosing the rotor was defined as a Rotating Domain, treated using the MRF. ω was specified based on the target TSR. The outer rectangular region remained a Stationary Domain, with its external faces modelled as no-slip walls to maintain confinement of the flow field.

Grid independence study

A grid independence study was conducted using three levels of mesh refinement coarse, medium, and fine across three element types: TET4 (linear tetrahedral), TET10 (quadratic tetrahedral), and TET15 (higher-order tetrahedral) as shown in Figure 5. The primary metric evaluated was the percentage of elements with a quality index above 0.75, ensuring both mesh fidelity and numerical stability. The quality index improved with increasing mesh resolution and element complexity. For coarse meshes, the quality index ranged from 0.81 (TET4) to 0.85 (TET15). Medium meshes showed a substantial improvement, with the TET10 configuration achieving the highest quality index of 0.95 at 1,209,765 elements. Further refinement to fine meshes provided negligible gains, with quality indices plateauing around 0.945–0.95, indicating that mesh convergence was achieved. Based on this trend, the medium-density mesh with TET10 elements was selected as the optimal configuration for subsequent computational simulations. This choice provided a balance between mesh quality and computational efficiency, ensuring reliable numerical results without excessive processing time.

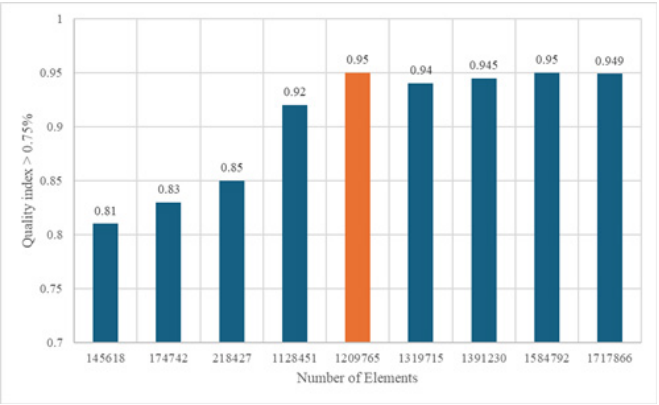


Figure 5: Variation of mesh quality index with the number of elements, demonstrating mesh convergence

Experimental setup and test conditions

The HAWT blade was fabricated using advanced 3D printing technology with polylactic acid (PLA) material for testing in the wind tunnel. PLA was selected as the printing material due to its excellent printability, adequate strength-to-weight ratio for small-scale applications, and good dimensional stability, which ensured that the airfoil geometry remained intact under the low Reynolds number testing conditions.

A 3-bladed HAWT prototype, with a rotor diameter of 350 mm (radius R=175 mm) and a constant pitch angle of 3°, was evaluated experimentally in a low-speed, open-circuit, suction-type wind tunnel. The schematic of the experimental setup is presented in Figure 6, while Figure 7 shows the physical test setup and electrical connections used for voltage measurement. The wind tunnel specifications and the experimental flow conditions are summarized in Table 2 and Table 3, respectively (Sergiienko et al., 2022). The experimental measurements were based on electrical output from the coupled generator system. The rotor rotational speed was measured using electrical output (voltage) was recorded. The support tower introduces blockage and flow interference, potentially affecting wake development and measured performance. Its relatively large diameter may contribute to minor deviations between CFD and experimental results. Future work will adopt slender supports and apply blockage correction to improve accuracy.

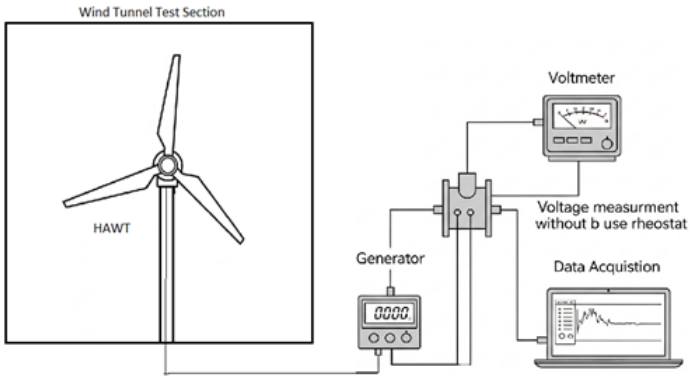
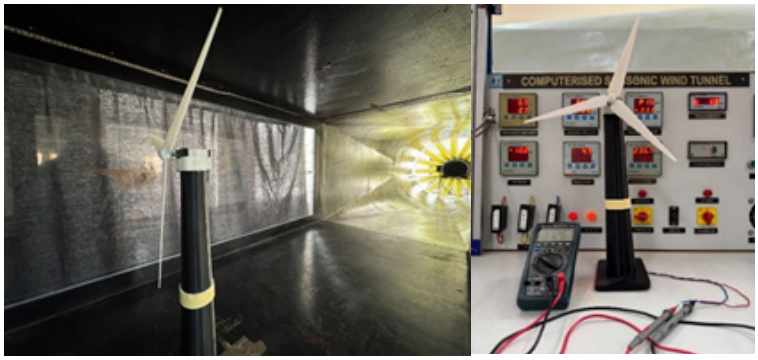


Figure 6: Schematic representation of the experimental setup for performance testing of the HAWT prototype



(a) (b)

Figure 7: HAWT (a) placed in wind tunnel and (b) connection for voltage measurement

Table 2: Specifications of the low-speed wind tunnel used for the experimental performance evaluation of the HAWT prototype

Parameter	Value
Wind Tunnel type	Low speed, open circuit, and suction type.
Test section size	Square cross section: 0.6m height, 0.6m width
Test section Length	2000 mm
Contraction ratio	9:1
Velocity range	0 to 50 m/sec
Max axial fan speed	1500 rpm
Drive	AC motor 20 Hp
Power requirement	AC, 3 Phase, 440 volts, 64 amps
Turbulence level	0.3% to 0.7%

Table 3: Experimental operating conditions used for performance testing of the HAWT prototype

Parameter	Value
Altitude	920 m above sea level
Freestream density (ρ_∞)	1.133 kg/m^3
Dynamic viscosity (μ_∞)	1.7e^{-5} Ns/m^2
Freestream velocity (V_∞)	2, 3, 4 and 5 m/sec
Reynolds number (Re)	3.9 ×10^4, 5.9 ×10^4, 7.9 ×10^4 and 9.9×10^4

RESULTS AND DISCUSSIONS

Table 4 presents the pressure contours at multiple spanwise sections of the wind turbine blade for various TSRs and blade deflection angles. These plots reveal the distribution of pressure around the blades, highlighting the primary lift mechanism. At all TSRs, a high-pressure region is seen on the lower surface (pressure side), while a low-pressure region forms on the upper surface (suction side). This pressure differential is more pronounced at higher TSRs and moderate blade deflection angles, suggesting improved lift and torque generation. The +10° deflection shows strong pressure gradients, indicating optimal aerodynamic performance under those conditions.

Table 5 illustrates velocity contours at spanwise sections of the blade under different TSRs and blade configurations. These contours show how the incoming flow accelerates around the blades due to energy extraction. A noticeable reduction in axial velocity immediately downstream of the rotor indicates the formation of a wake. The highest reduction occurs at TSR 7, consistent with more effective energy extraction. Additionally, tip vortices are visible as high-speed zones near the blade tips, confirming the presence of strong rotational flow and secondary flow structures. The degree of velocity recovery downstream provides insights into wake development and flow reattachment.

Table 6 illustrates turbulent kinetic energy contours, which represent zones of high turbulence intensity caused by blade–fluid interaction. Higher TKE values are predominantly observed in the wake region, especially behind the blade tips, where strong vortices and shear layers form. Among the configurations, the +10° and +15° deflection blades at TSR 6 and 7 generate the most intense turbulence, likely due to more aggressive flow detachment and stronger vortex structures. The increased TKE signifies energy dissipation and enhanced mixing, which can influence downstream turbine performance in wind farms (wake interference).

Table 7 depicts surface pressure distributions on the blade surfaces under different operating conditions. These visuals help identify regions of high and low pressure across the blade surface. For all configurations, strong suction (low pressure) appears near the leading edge on the suction side, especially in the mid-span to tip region. The highest-pressure differentials occur with +10° deflection blades at TSR 6 and 7, indicating enhanced lift. The figures also show more uniform pressure distribution at optimal TSRs, which supports the turbine's efficiency and reduced flow separation.

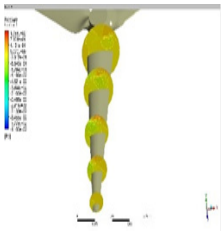
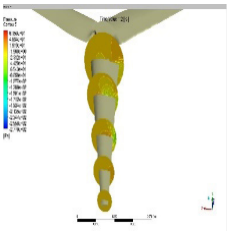
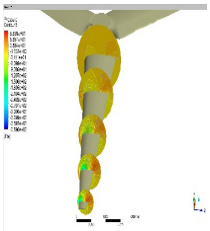
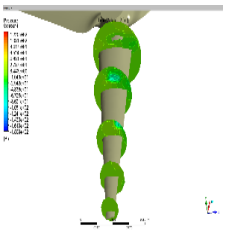
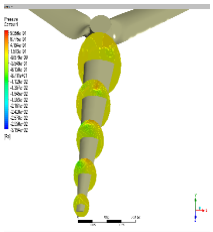
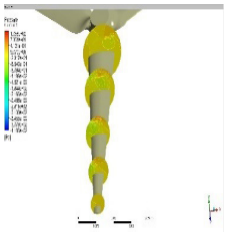
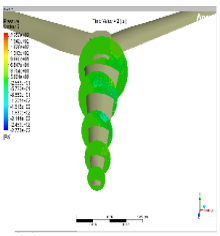
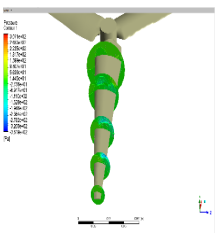
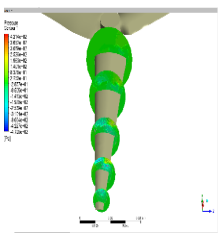
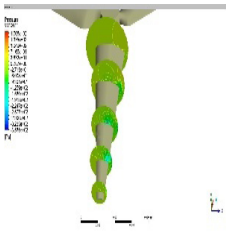
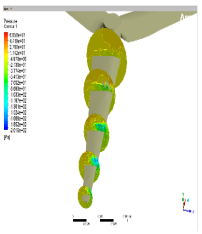
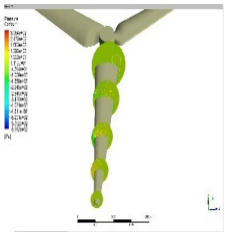
Table 8 illustrates surface streamlines to provide a visual representation of flow adherence and direction on the blade surfaces. For TSRs 5 through 7, most configurations show attached flow along the blade span, particularly at +5° and +10° deflections. Minor flow separation is evident near the root and at the trailing edge, especially for the +15° deflection at higher TSRs. The helical pattern of the streamlines confirms the rotational nature of the flow and efficient momentum transfer from the wind to the rotor. This figure is crucial in validating blade design effectiveness in maintaining attached flow and minimizing stall.

The present study compares the numerical and experimental evaluation of the coefficient of power (C_p) for a HAWT equipped with passive trailing edge morphing at various deflection angles (+5°, +10°, and +15°) under low Reynolds number conditions as shown in Figure 8. The blade geometry is based on a NACA 2412 profile, and the morphing is applied over 50% of the chord length from the trailing edge. The results are analyzed for a range of TSR from 2.0 to 8.0 for both the conventional straight blade and the morphing configurations. A clear trend is observed wherein C_p increases with increasing TSR up to a certain point, after which it begins to decline, consistent with the characteristic power-coefficient behaviour reported for small-scale wind turbines operating at low Reynolds numbers, where rotational speeds beyond the optimum tip speed ratio increase profile drag and promote earlier flow separation (Kulak et al., 2024; Sudhamshu et al., 2016). Furthermore, the addition of trailing edge deflection significantly enhances the C_p across most TSRs, with +15° deflection yielding the highest performance both numerically and experimentally, in agreement with the general finding that increasing trailing-edge camber through morphing or flap deflection raises the power coefficient of small-scale wind turbine rotors (Ali et al., 2021; Giammichele et al., 2024; Mansi & Aydin, 2022). This confirms the aerodynamic benefit of morphing in enhancing lift and delaying separation, thus improving turbine efficiency.

Comparing numerical predictions with experimental measurements, the overall variation in C_p is within ±10%, which is generally acceptable given the inherent limitations in replicating exact conditions in CFD and wind tunnel experiments, and is comparable to the numerical-experimental deviation reported for other trailing-edge-flap-equipped small-scale HAWTs evaluated under similarly low wind speeds (Yin et al., 2024). For instance, at TSR 6.0, the numerical C_p for +15° deflection is 0.5075, while the experimental C_p is slightly higher at 0.5252, resulting in a percentage difference of approximately 3.5%. At lower TSR values, such as 3.0, a slight underprediction is observed in experiments compared to simulation, possibly due to laminar-to-turbulent transition not being fully captured in the wind tunnel or unsteady wake interactions not accounted for in the steady numerical model, an effect consistent with the strong sensitivity of measured performance to transition location previously reported for low-Reynolds-number airfoils (Kassa et al., 2024).

The mismatch between numerical and experimental results can be attributed to several factors. Firstly, the numerical model assumes ideal surface finish and perfect geometry, while experimental blades may have slight manufacturing tolerances, surface roughness, or minor asymmetries. Secondly, the CFD simulations may use turbulence models (such as SST k-ω) that do not fully capture laminar separation bubbles or transition zones, which are especially significant at low Reynolds numbers, a limitation also highlighted in comparative turbulence-model assessments for rotor aerodynamics (Daróczy et al., 2015). Thirdly, wind tunnel blockage effects, support interference, and instrumentation errors may introduce discrepancies in experimental measurements. Additionally, the simplified assumption of 2D or quasi-3D simulations in numerical analysis may fail to fully represent the 3D nature of flow near blade tips, where vortex formation and induced drag play a more dominant role.

Table 4: Pressure contours across the blade sections under different trailing-edge morphing deflections

Blade	TSR 5	TSR 6	TSR 7
Straight blade			
+5° deflection blade			
+10° deflection blade			
+15° deflection blade			

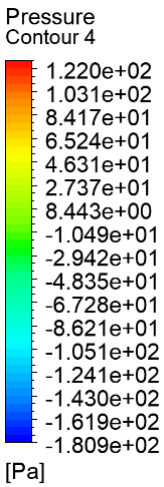
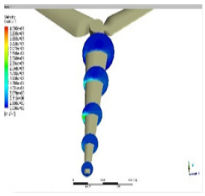
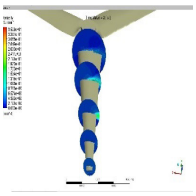
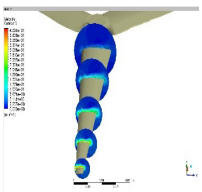
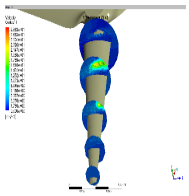
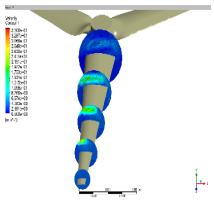
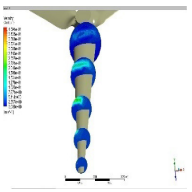
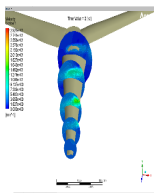
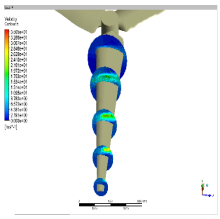
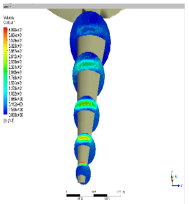
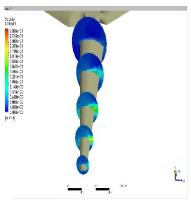
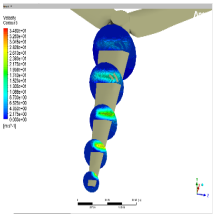
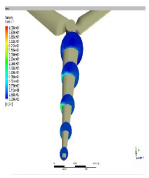


Table 5: Velocity contours across the blade sections under different trailing-edge morphing deflections

Blade	TSR 5	TSR 6	TSR 7
Straight blade			
+5° deflection blade			
+10° deflection blade			
+15° deflection blade			

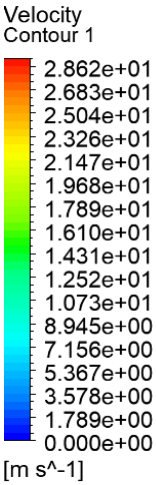
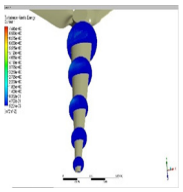
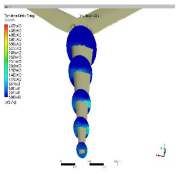
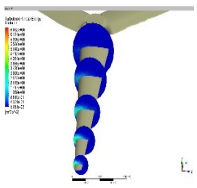
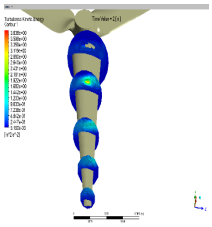
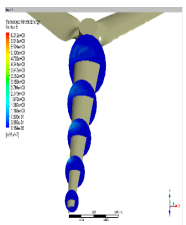
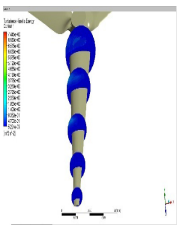
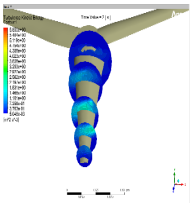
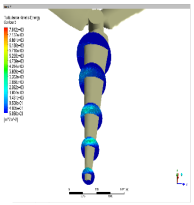
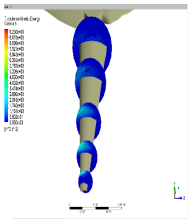
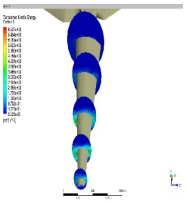
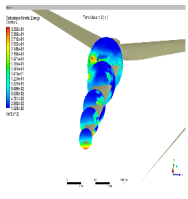
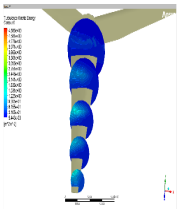


Table 6: Turbulent Kinetic Energy (TKE) contours across the blade sections under different trailing-edge morphing deflections

Blade	TSR 5	TSR 6	TSR 7
Straight blade			
+5° deflection blade			
+10° deflection blade			
+15° deflection blade			

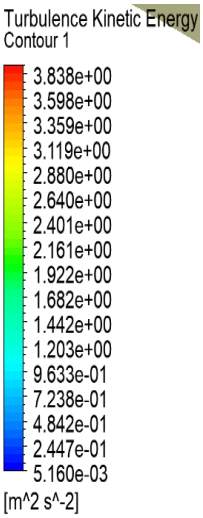
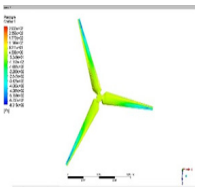
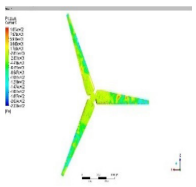
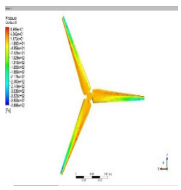
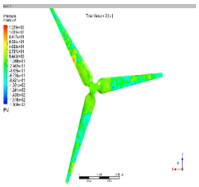
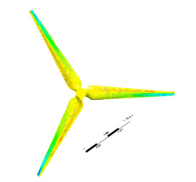
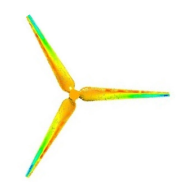
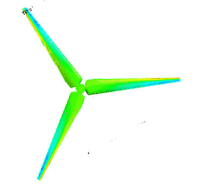
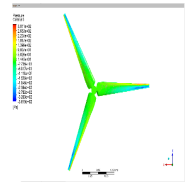
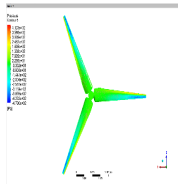
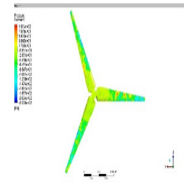
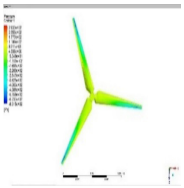


Table 7: Surface Pressure Contour on Blades under different trailing-edge morphing deflections

Blade	TSR 5	TSR 6	TSR 7
Straight blade			
+5° deflection blade			
+10° deflection blade			
+15° deflection blade			

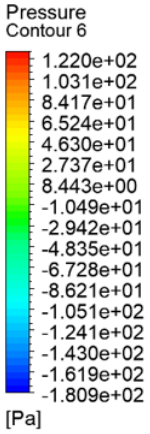
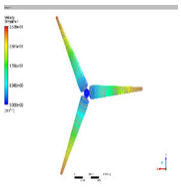
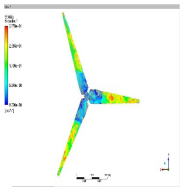
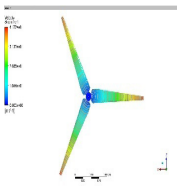
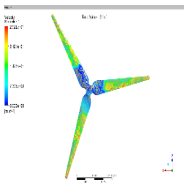
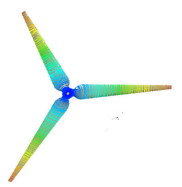
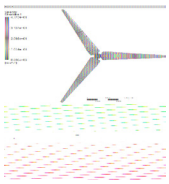
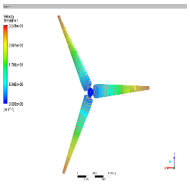
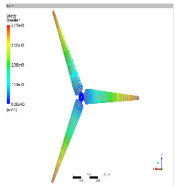
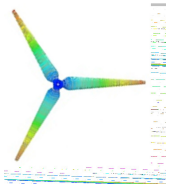
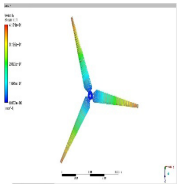
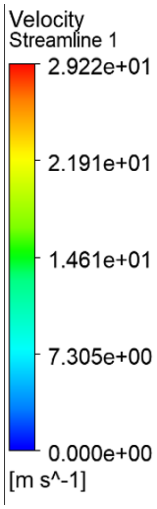


Table 8: Streamline Visualization on Blade Surface under different trailing-edge morphing deflections

Blade	TSR 5	TSR 6	TSR 7
Straight blade			
+5° deflection blade			
+10° deflection blade			
+15° deflection blade			



From a performance perspective, the morphing blades show substantial improvements over the straight blades. For example, at TSR 6.0, the experimental C_p of the +15° deflected blade is 0.5252, compared to 0.3586 for the straight blade, which translates to a 46.5% performance gain. Even a moderate deflection of 10° yields a significant increase (~26.4%). This magnitude of enhancement agrees, in trend, with previous studies on trailing-edge morphing and flap devices for small-scale wind turbines, although the absolute gains reported in the literature vary considerably depending on the deflection angle and chordwise extent of the morphed or hinged region. The present enhancement is closely comparable to that reported by (Ali et al., 2021), who observed power augmentations of up to 53% for a morphed trailing edge on a small-scale wind turbine, with the largest gains occurring under low-wind, low-TSR-equivalent conditions like those examined here. In contrast, the present gains are considerably higher than the 8.3% (BEM) to 12% (3D CFD) power coefficient increase reported by (Mansi & Aydin, 2022) for a fixed trailing-edge flap at TSR 7.0, and the 15.24% increase reported by (Yin et al., 2024) for an optimum morphed trailing-edge flap deflected by only 3° on the NREL Phase II wind turbine at a comparable tip speed ratio (TSR ≈ 5.95). This difference is attributed primarily to the larger deflection angle used in the present study (up to +15°, versus 3° in (Yin et al., 2024)) and the greater chordwise extent of the morphed region (50% of the local chord, compared with the 20-30% typically employed in the literature), both of which increase the effective camber and lift generated over a larger portion of the blade, consistent with the established dependence of trailing-edge-flap performance gains on deflection magnitude and flap chord fraction (Zhuang et al., 2020). Taken together, these comparisons indicate that the direction and general scale of the present findings agree with earlier work, while the specific magnitude of the improvement reflects the more aggressive morphing configuration adopted here relative to most previous studies. These findings demonstrate that trailing edge morphing can be a promising approach to enhance aerodynamic efficiency in small-scale wind turbines, particularly in environments where the flow is less energetic and prone to early separation. Although the +15° deflection configuration demonstrates the highest performance within the tested range, adopting a fixed geometry may lead to suboptimal performance under varying wind conditions. Morphing provides the flexibility to dynamically adjust blade camber, thereby optimizing performance across a wider range of operating conditions, which is essential for real-world wind energy applications.

The present study focuses on aerodynamic performance at low wind speeds; however, its implications for annual energy production (AEP) can be inferred. AEP depends on both the turbine efficiency and the wind speed distribution (Manwell et al., 2010). The results show consistent improvement in the coefficient of power (C_p) for morphing configurations within the 2–5 m/s range, which is commonly encountered in low-wind environments. Even modest gains in C_p at these speeds can significantly enhance overall energy yield. The +15° deflection exhibits the best performance, indicating strong potential for improved energy capture under low wind conditions. However, higher camber may increase drag at elevated wind speeds, limiting its effectiveness beyond the tested range. Therefore, while fixed morphing improves low-speed performance, adaptive morphing is more suitable for maximizing AEP under varying wind conditions. A detailed AEP analysis using site-specific wind data is recommended for future work.

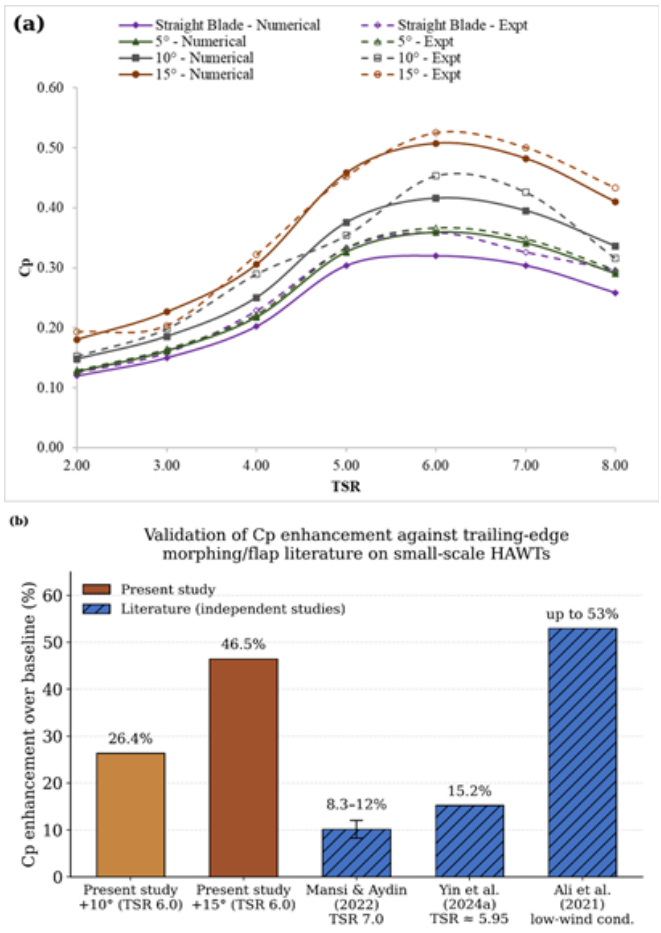


Figure 8: Figure 8: (C_p)–TSR curves for straight and trailing-edge-morphed blades (+5°, +10°, +15°): (a) numerical and experimental results; (b) comparison of (C_p) enhancement at TSR 6.0 with published data (Ali et al., 2021; Mansi & Aydin, 2022; Yin et al., 2024)

CONCLUSION

This study successfully investigated the efficacy of passive trailing edge morphing, specifically with 50% chord deflection, in enhancing the aerodynamic performance and efficiency of HAWT blades under low Reynolds number conditions. Through a comprehensive approach combining CFD simulations and experimental wind tunnel testing of a NACA 2412-based prototype, the impact of various deflection angles (+5°, +10°, and +15°) was meticulously evaluated. The findings conclusively demonstrate that the application of passive trailing edge morphing significantly improves the turbine's coefficient of power across the tested TSR range. Notably, the 15-degree deflection configuration

consistently yielded the highest performance, both in numerical predictions and experimental measurements, highlighting its effectiveness in optimizing the blade's aerodynamic profile. A substantial performance gain of up to 46.5% in C_p was observed for +15° deflected blade compared to the conventional straight blade at optimal TSR, underscoring the considerable benefits of camber control. This study demonstrates substantial aerodynamic improvements with the proposed trailing-edge morphing configuration, confirming its potential for enhancing the performance of small-scale wind turbines. The close agreement between numerical and experimental results (generally within 10% variation) validates the accuracy of the computational model while acknowledging inherent discrepancies attributed to idealizations in CFD and experimental factors. This research underscores the considerable potential of passive trailing edge morphing as a promising technology for augmenting the aerodynamic efficiency of small-scale HAWTs, particularly in environments prone to low wind speeds and viscous flow phenomena where traditional fixed-geometry blades often struggle. The insights gained are crucial for developing adaptive blade designs capable of maintaining optimal performance across fluctuating operational conditions. Future work should focus on exploring dynamic morphing strategies, optimizing the chord-wise and span-wise distribution of deflection, and investigating the practical integration of actuation mechanisms into full-scale prototypes. Further scope should be on implementing active trailing edge morphing for very low Reynolds number flows.

ACKNOWLEDGEMENTS

The authors acknowledge Nitte (Deemed to be University), Nitte Meenakshi Institute of Technology, Bengaluru 560064, Karnataka, India, for providing institutional facilities and support for this research.

DECLERATION OF CONFLICTS OF INTEREST

The authors declare no conflict of interest.

FUNDING INFORMATION

No funding was received for this research.

AUTHOR CONTRIBUTIONS

Conceptualization, Methodology, Software, Validation, Formal analysis, Data curation, Project administration, Supervision: **S.P.K.;** Formal analysis, Investigation, Visualization: **K.A.R., A.A.;** Writing – original draft, writing – review and editing: **S.P.K.**

DATA AVAILABILITY STATEMENT

The authors confirm that the data supporting the findings of this study are available within the article.

REFERENCES

Ajaj, R. M., Beaverstock, C. S., & Friswell, M. I. (2016) Morphing aircraft: The need for a new design philosophy, *Aerospace Science and Technology*, **49**, 154–166. https://doi.org/10.1016/j.ast.2015.11.039

Akhter, M. Z., Ali, A. R., Jawahar, H. K., Omar, F. K., & Elnajjar, E. (2023) Performance enhancement of small-scale wind turbine featuring morphing blades, *Energy*, **278**, 127772. https://doi.org/10.1016/j.energy.2023.127772

Akhter, M. Z., & Omar, F. K. (2021) Review of Flow-Control Devices for Wind-Turbine Performance Enhancement, *Energies*, **14**, (5), 1268. https://doi.org/10.3390/en14051268

Ali, A. R., Akhter, M. Z., & Omar, F. K. (2021) Performance enhancement of a small-scale wind turbine featuring morphed trailing edge, *Sustainable Energy Technologies and Assessments*, **46**, 101229. https://doi.org/10.1016/j.seta.2021.101229

Ameduri, S., & Concilio, A. (2020) Morphing wings review: aims, challenges, and current open issues of a technology, *Proceedings of the Institution of Mechanical Engineers, Part C: Journal of Mechanical Engineering Science*, **237**, 4112–4130. https://doi.org/10.1177/0954406220944423

Apata, O., & Oyedokun, D. T. O. (2020) An overview of control techniques for wind turbine systems, *Scientific African*, **10**, e00566. https://doi.org/10.1016/j.sciaf.2020.e00566

Arunvinthan, S., Raatan, V. S., Nadaraja Pillai, S., Pasha, A. A., Rahman, M. M., & Juhany, K. A. (2021) Aerodynamic characteristics of shark scale-based vortex generators upon symmetrical airfoil, *Energies*, **14**, (7). https://doi.org/10.3390/en14071808

Barbarino, S., Bilgen, O., Ajaj, R. M., Friswell, M. I., & Inman, D. J. (2011) A Review of Morphing Aircraft, *Journal of Intelligent Material Systems and Structures*, **22**, (9), 823–877. https://doi.org/10.1177/1045389X11414084

Bi, K., Sun, W., & Zhang, Z. (2020) Bio-inspired morphing wings: A review, *Aerospace Science and Technology*, **100**, 105740. https://doi.org/10.1016/j.ast.2020.105740

Burdett, T. A., & Van Treuren, K. W. (2012) Scaling Small-Scale Wind Turbines for Wind Tunnel Testing, *Volume 6: Oil and Gas Applications; Concentrating Solar Power Plants; Steam Turbines; Wind Energy*, 811–820. https://doi.org/10.1115/GT2012-68359

Chen, H., & Qin, N. (2017) Trailing-edge flow control for wind turbine performance and load control, *Renewable Energy*, **105**, 419–435. https://doi.org/10.1016/j.renene.2016.12.073

Cheng, G., Ma, T., Yang, J., Chang, N., & Zhou, X. (2023) Design and experiment of a seamless morphing trailing edge, *Aerospace*, **10**, (3). https://doi.org/10.3390/aerospace10030282

Clements, D., & Djidjeli, K. (2023) Aerodynamic Performance of Morphing and Periodic Trailing-Edge Morphing Airfoils in Ground Effect, *Journal of Aerospace Engineering*, **36**, (3), 4023012. https://doi.

org/10.1061/JAEEEZ.ASENG-4707

Daróczy, L., Janiga, G., Petrasch, K., Webner, M., & Thévenin, D. (2015) Comparative analysis of turbulence models for the aerodynamic simulation of H-Darrieus rotors, *Energy*, **90**, 680–690. https://doi.org/10.1016/j.energy.2015.07.102

Douglas, F. H., Jackson, T. R., & James, J. J. (2019) Geometric Definition and Ideal Aerodynamic Performance of Parabolic Trailing-Edge Flaps, *International Journal of Astronautics and Aeronautical Engineering*, **4**, 26. https://doi.org/10.35840/2631-5009/7526

Giammichele, L., D'Alessandro, V., Falone, M., & Ricci, R. (2024) Experimental assessment of a morphing trailing edge device for wind turbine blade performance improvement, *Journal of Renewable and Sustainable Energy*, **16**, (1), 013306. https://doi.org/10.1063/5.0174768

Huang, X., Alavi Moghadam, S. M., Meysonnat, P. S., Meinke, M., & Schröder, W. (2019) Numerical analysis of the effect of flaps on the tip vortex of a wind turbine blade, *International Journal of Heat and Fluid Flow*, **77**, 336–351. https://doi.org/10.1016/j.ijheatfluidflow.2019.05.004

Kan, Z., LI, D., Xiang, J., & Cheng, C. (2020) Delaying stall of morphing wing by periodic trailing-edge deflection, *Chinese Journal of Aeronautics*, **33**, (2), 493–500. https://doi.org/10.1016/j.cja.2019.09.028

Kassa, B. Y., Baheta, A. T., & Beyene, A. (2024) Aerodynamic performance characteristics of low Re airfoils: A parametric and multi criteria decision study, *Results in Engineering*, **24**, 103174. https://doi.org/10.1016/j.rineng.2024.103174

Kaul, U. K., & Nguyen, N. T. (2015) A 3-D computational study of a variable camber continuous trailing edge flap (VCCTEF) spanwise segment, *33rd AIAA Applied Aerodynamics Conference*, 1–20. https://doi.org/10.2514/6.2015-2422

Khedr, A. (2025) Bio-mimicry in the aerodynamics of small horizontal axis wind turbines, *Sustainable Energy Technologies and Assessments*, **76**, 104260. https://doi.org/10.1016/j.seta.2025.104260

Kodigaddi, S. P. (2026) Structural assessment and experimental validation of a hybrid composite–polymer trailing-edge morphing wing for low-Reynolds-number UAVs, *Journal of Engineering and Applied Science*, **73**, (1), 247. https://doi.org/10.1186/s44147-026-01106-3

Kodigaddi, S. P., Badardinni, R., Hosur, S., & Manvi, P. (2022) The Effect of Deflection Angle on Aerodynamic Characteristics of Morphing Trailing Edge Airfoil at Low Speed, *AIP Conference Proceedings*, 30003. https://doi.org/10.1063/5.0116412

Kodigaddi, S. P., Joshi, S. S., & Musthafa, R. (2026) CFD & experimentally validated quasi-static trailing-edge morphing-inspired configurations for aerodynamic enhancement of vertical axis wind turbines, *Journal of Engineering and Applied Science*, **73**, (1), 354. https://doi.org/10.1186/s44147-026-01213-1

Kodigaddi, S. P., Manvi, P., & Sharma, R. (2026) Comparative structural evaluation of polymer-based morphing wing ribs using finite element analysis for optimized adaptive aerospace applications, *Journal of Engineering and Applied Science*, **73**, (1), 109. https://doi.org/10.1186/s44147-026-00971-2

Kodigaddi, S. P., & Venkataramana, S. H. (2025) Experimental and Numerical Study on Optimization of Zigzag Rib Topologies for Trailing-Edge Morphing Wings for Low-Speed Applications, *Journal of Aerospace Technology and Management*, **17**. https://doi.org/10.1590/jatm.v17.1400

Kodigaddi, S. P., Venkataramana, S. H., Natesan, K., & Mazlan, N. (2025) Experimental Investigation on a Trailing Edge Morphing Airfoil (TEMA) with Zigzag Rib Structure at Low Speed, *Pertanika Journal of Science and Technology*, **33**, (1), 195–217. https://doi.org/10.47836/pjst.33.1.09

Kulak, M., Lipian, M., Olasek, K., Pereira, M., & Ravelet, F. (2024) Rotor solidity and blade pitch influence on horizontal axis small wind turbine performance – Experimental study, *Energy Reports*, **12**, 4568–4577. https://doi.org/10.1016/j.egyr.2024.10.036

Li, C., Pan, T., Li, T., Zheng, M., Li, Q., & Dowell, E. H. (2025) Aerodynamic Behavior of a Wind Turbine Under Blade Pitching Motion, *American Institute of Aeronautics and Astronautics*, **63**, (4), 1368–1381. https://doi.org/10.2514/1.J063926

Li, L. J., & He, Z. L. (2023) Dynamic mode decomposition analysis of flow separation control on wind turbine airfoil using leading-edge rod, *Energy*, **268**, 126588. https://doi.org/10.1016/j.energy.2023.126656

Maguire, J. M., Mamalis, D., Ōtomo, S., & McCarthy, E. D. (2024) Passively morphing trailing edge design for composite tidal turbine blades, *Composite Structures*, **337**. https://doi.org/10.1016/j.compstruct.2024.118090

Mane, R., Bhatia, K., Sharma, S., & Prasad, R. K. (2025) A CFD Analysis of the Geometrical Optimization of Slotted Airfoils by Using the RANS k-ω; SST Turbulence Model, *Journal of Aerospace Engineering*, **38**, (2), 4024118. https://doi.org/10.1061/JAEEEZ.ASENG-5906

Mansi, A., & Aydin, D. (2022) The impact of trailing edge flap on the aerodynamic performance of small-scale horizontal axis wind turbine, *Energy Conversion and Management*, **256**, 115396. https://doi.org/10.1016/j.enconman.2022.115396

Manwell, J. F., McGowan, J. G., & Rogers, A. L. (2010) Wind energy explained: Theory, design and application, https://doi.org/10.1002/9781119994367

Mohammadi, M., & Maghrebi, M. J. (2020) Aerodynamic performance enhancement of horizontal axis wind turbines by dimples on blades: Numerical investigation, *Energy*, **195**, 116972. https://doi.org/10.1016/j.energy.2020.117056

Mowla, Md. N., Asadi, D., Durhasan, T., Jafari, J. R., & Amoozgar, M. (2025) Recent advancements in morphing applications: Architecture, artificial intelligence integration, challenges, and future trends-a comprehensive survey, *Aerospace Science and Technology*, **161**, 110102. https://doi.org/10.1016/j.ast.2025.110102

Nabhani, A., Tousi, N. M., Coma, M., Bugeda, G., & Bergadà, J. M. (2025) Large-scale horizontal axis wind turbine aerodynamic efficiency optimization using active flow control and synthetic jets, *Energy*, **319**. https://doi.org/10.1016/j.energy.2025.134940

O'Brien, J. M., Young, T. M., O'Mahoney, D. C., & Griffin, P. C. (2017) Horizontal axis wind turbine research: A review of commercial CFD, FE codes and experimental practices, *Progress in Aerospace Sciences*, **92**, 1–24. https://doi.org/10.1016/j.paerosci.2017.05.001

Parancheerivilakkathil, M. S., Pilakkadan, J. S., Ajaj, R. M., Amoozgar, M., Asadi, D., Zweiri, Y., & Friswell, M. I. (2024) A review of control strategies used for morphing aircraft applications, *Chinese Journal of Aeronautics*, **37**, (4), 436–463. https://doi.org/10.1016/j.cja.2023.12.035

Roslan, S. A. H., Rasid, Z. A., & Ehsan, A. K. A. M. (2022) The Aerodynamic Performance of the Small-Scale Wind Turbine Blade with NACA0012 Airfoil, *CFD Letters*, **14**, (10), 87–98. https://doi.org/10.37934/cfdl.14.10.8798

Saemian, M., & Bergadà, J. M. (2025) Active flow control actuators on wind turbines; comprehensive review, *Ocean Engineering*, **339**, 121991. https://doi.org/10.1016/j.oceaneng.2025.121991

Sergiienko, N. Y., da Silva, L. S. P., Bachynski-Polić, E. E., Cazzolato, B. S., Arjomandi, M., & Ding, B. (2022) Review of scaling laws applied to floating offshore wind turbines, *Renewable and Sustainable Energy Reviews*, **162**, 112477. https://doi.org/10.1016/j.rser.2022.112477

Somashekar, V., & Immanuel Selwynraj, A. (2022) Aerodynamic study of low Reynolds number airfoil and mini-unmanned aerial vehicle in simulated rain environment, *Aircraft Engineering and Aerospace Technology*, **94**, (10), 1748–1758. https://doi.org/10.1108/AEAT-12-2021-0379

Sudhamshu, A., Pandey, M. C., Sunil, N., N.S., S., Mugundhan, V., & Velamati, R. K. (2016) Numerical study of effect of pitch angle on performance characteristics of a HAWT, *Engineering Science and Technology, an International Journal*, **19**, (1), 632–641. https://doi.org/10.1016/j.jestch.2015.09.010

Temesgen Terefa, G., Githu Njiri, J., Irungu Muiruri, P., & Merga Abdissa, C. (2025) Optimal design and analysis of a mixed airfoil blade for small-scale HAWTs, *Engineering, Technology & Applied Science Research*, **15**, (3), 22538–22547. https://doi.org/10.48084/etasr.10275

Tummala, A., Velamati, R. K., Sinha, D. K., Indraja, V., & Krishna, V. H. (2016) A review on small scale wind turbines, *Renewable and Sustainable Energy Reviews*, **58**, 1189–1207. https://doi.org/10.1016/j.rser.2015.12.027

Wang, R., Ma, X., Zhang, G., Ying, P., & Wang, X. (2023) Numerical Simulation of Continuous Morphing Wing with Leading Edge and Trailing Edge Parabolic Flaps, *Journal of Aerospace Engineering*, **36**, (5), 4023051. https://doi.org/10.1061/JAEEEZ.ASENG-4622

Yan, B., Li, Y., Dai, P., & Liu, S. (2019) Aerodynamic Analysis, Dynamic Modeling, and Control of a Morphing Aircraft, *Journal of Aerospace Engineering*, **32**, (5), 4019058. https://doi.org/10.1061/(ASCE)AS.1943-5525.0001047

Yin, R., Xie, J.-B., & Yao, J. (2024) Numerical and experimental study of the effect of an innovative trailing-edge flap on the aerodynamic performance of small-scale horizontal-axis wind turbines, *Wind Engineering*, **48**, (6), 999–1011. https://doi.org/10.1177/0309524X241268919

Zhuang, C., Yang, G., Zhu, Y., & Hu, D. (2020) Effect of morphed trailing-edge flap on aerodynamic load control for a wind turbine blade section, *Renewable Energy*, **148**, 964–974. https://doi.org/10.1016/j.renene.2019.10.082